Wang, Z., Kusky, T.M., and Wang, L., 2022, Long-lasting viscous drainage of eclogites from the cratonic lithospheric mantle after Archean subduction stacking: Geology, https://doi.org/10.1130/G49793.1

Methods and supplementary information: Long-lasting Viscous drainage of eclogites from the cratonic lithospheric mantle after Archean subduction stacking

Zhensheng Wang [1, *], Timothy M. Kusky [1, 2 *], Lu Wang [1]

1. *State Key Lab of Geological Processes and Mineral Resources, Center for Global Tectonics, School of Earth Sciences, China University of Geosciences, Wuhan, China*
2. *Three Gorges Research Center for Geohazards, China University of Geosciences, Wuhan, China*

**Corresponding author: jasonwang@cug.edu.cn tkusky@gmail.com*

Methods

Governing equations

The dynamic processes in the models are implemented via underworld2 (Moresi et al., 2003). It tracks the properties of materials via a particles embedded in cell method and governs the system via the conservation of mass, momentum and energy as shown below:

$$\nabla \cdot u = 0 \quad (1)$$

$$\nabla[-PI + \eta(\nabla u + (\nabla u)^T)] = F_b \quad (2)$$

$$\frac{\partial T}{\partial t} + u\nabla T = \kappa\nabla^2 T - \frac{\alpha u_y g T}{Cp} + \frac{Q}{\rho Cp} \quad (3)$$

where, u the velocity, P the pressure, T the temperature, η the viscosity, F_b the buoyancy, ρ the density, g the gravitational acceleration, C_p the specific heat, t the time, κ the coefficient of thermal conductivity, α the coefficient of thermal expansion, u_y the vertical component of velocity, and Q the radiogenic heating, which can be simplified as a total decay process of all the radioactive elements (Turcotte and Schubert, 2002).

$$Q = 0.5^{\frac{(t-2500\ Myr)}{\tau}} Q_{present} \quad (4)$$

W

here $Q_{present}$ the present radiogenic heating value, t the model time, τ the half life of total radiogenic heating, τ=3000 Myr is used in all the models here (Turcotte and Schubert, 2002).

Rheology

For the mantle peridotites, we used a non-linear visco-plastic rheology, as shown below:

$$\eta = \min(\eta_{vis} + \eta_{plastic}) \qquad (5)$$

As for the plastic rheology, a simplified pressure-dependent Mohr-Coulomb yield criterion is used (Ranalli, 1995):

$$\eta_{plastic} = \frac{C_0 + C_1 P}{2\dot{\varepsilon}_{II}} \qquad (6)$$

Before the collision, a hydrous layer is adopted on the top 30 km of the slab domain to lubricate the stacking interface to maintain the subduction. For materials not in this layer, C_1 is set to 0.6. For materials in this layer, a strain weaking effect is taken into account via:

$$C_1 = \begin{cases} 0.012 & if\ \varepsilon \geq 0.02 \\ 0.6 & if\ \ \varepsilon < 0.02 \end{cases} \qquad (7)$$

In the post-stacking stage, C_1 in all the model domains is set to 0.6, so as to observe the evolution of eclogites with realistic cratonic rock rheological properties.

For the viscous rheology, we used a composite viscosity considering diffusion creep (η_{diff}), dislocation creep (η_{dis}) and influence of melt depletion degree (F, in %) (Capitanio et al., 2020).

$$\eta_{vis} = \left(\frac{1}{\eta_{diff}} + \frac{1}{\eta_{disl}}\right)^{-1} (1 - 0.0135F)^{-2.5} \exp(0.057F) \qquad (8)$$

The diffusion and dislocation creep are defined as functions of the pressure (P), temperature (T), composition (A) and second invariant of the strain rate tensor ($\dot{\varepsilon}_{II}$) (Table S1) (Hirth and Kohlstedt, 2003), f is a strength factor induced by fluids, partial melting, strain weakening, recrystallization or other mechanisms:

$$\eta_{diff,disl} = A\dot{\varepsilon}_{II}^{\frac{1-n}{n}} \exp\left(\frac{E + PV}{nRT}\right) f \qquad (9)$$

We tested different values of f (0.01-1.0), so as to test the influences of melts or fluids, and other weakening effects on the evolution of CLM eclogites.

For crustal eclogites and other rocks (Jin et al., 2002; Zhang and Green, 2007), only plastic rheology and dislocation creep are taken into account in related model domains, which means $\eta_{vis}=\eta_{dis}$ (Table S1). The dislocation creep of eclogites are based on experiments (Jin et al., 2002). The viscosity (Table S1) change between gabbro and eclogite in all the models takes place at ~45 km depth, so as to simulate the influences of eclogitization and its inverse transition.

Density

The density of mantle materials is a function of T, depth, reference density $\rho_{ref(depth)}$ (Fig. S1A) and depletion degree (*F*):

$$\rho = \rho_{ref(depth)}\left(1-\alpha\left(T-T_{present\_adiabat}\right)\right)-\Delta\rho_{(T,P,F)} \quad (10)$$

$$\Delta\rho_{(T,P,F)} = \left(\rho_{stp(F=0)}-\rho_{stp(F=F)}\right)\left(1-\alpha\left(T-T_{stp}\right)\right)\left(1+\beta\left(P-P_{stp}\right)\right) \quad (11)$$

where α is the thermal expansivity, β the compressibility coefficient. $\rho_{stp(F)}$ is the density measured under standard temperature (T_0) and pressure(P_0) (STP) condition and is a function of melt depletion degree (*F*).

The density of mantle peridotites under STP condition ($\rho_{stp(F)}$) can be described as a monotonic function of Mg# in olivine and depletion degree (*F*) (Fig. S1B-C) (Bernstein et al., 2007; Lee, 2003).

The $\rho_{ref(depth)}$ profiles of mantle and mafic crust are based on physical and geophysical constraints (Xu et al., 2008; Yan et al., 2020), in which the eclogitization and other main phase transitions are taken into account via density changing with depth (Fig. S1A). The $\Delta\rho_{(F)}$ in Eq. 10 and 11 is equal to 0 for eclogites.

The density of upper crust follows the commonly used density function:

$$\rho = \rho_0\left(1-\alpha(T-273.15)\right)\left(1+\beta(P-0)\right) \quad (12)$$

Thermal conditions

Initial temperature distribution in the ambient mantle, crust thickness and oceanic lithosphere depletion degree

The initial temperature in the ambient mantle follows the mantle adiabat profile (Rodríguez González et al., 2012):

$$T_{ambient} = T_L \exp\left(\frac{g\alpha}{Cp} * (depth - L)\right) + 273.15 + \Delta Tp \quad (13)$$

where T_L =1350 ºC, L=100,000 m, depth is in m, ΔTp the difference between mantle potential temperature in Archean and that at present. The thermal state of mantle in the Archean is demonstrated to be hotter than the present one, as shown by estimations of the mantle potential temperature (Tp) of that time (Herzberg et al., 2010). Different degrees of mantle potential temperature differences (ΔTp = 135-250 K) are constrained according to different data sets or criteria (Aulbach and Arndt, 2019; Ganne and Feng, 2017; Herzberg et al., 2010). Despite these divergences and the secular cooling in the Archean, we test different values (ΔTp= 135, 200, 250 K) in different model setups. A first-order linear secular cooling (with different cooling rates, λ=-ΔTp / 2500 Myr) is used in our models via temperature change at the bottom boundary (Wang et al., 2018).

The ambient mantle temperature influences the degree and distribution of partial melting below the mid-ocean ridge. Thus, it also influences the thickness of the oceanic crust and the depletion degree and thickness of the depleted peridotitic mantle layer. A simple integral of partial melting degree along the ambient mantle geothermal profile is used to calculate the approximate thickness of the oceanic crust in the Archean:

$$thickness_{crust} = \int_{bottom}^{top} \varphi \, d_{depth} \quad (14)$$

where φ the partial melting degree along the ambient mantle geothermal profile, calculated using methods by Katz et al. (2003). According to this equation, the thickness of the oceanic crust in Archean can range from 17.3-37.7 km, corresponding to ΔTp=135-250 K. This is approximately consistent with the estimation (<~30-45 km) by Herzberg and Rundnick (2012). The thickness and depletion degree (vs. depth) of the oceanic mantle lithosphere is calculated using the same partial melting methods (Katz et al., 2003).

Accordingly, a higher Tp can lead to thicker oceanic crust and depleted mantle lithosphere with larger depletion degree, which can finally influence eclogite evolution in the CLM.

Initial temperature distribution in the lithosphere

For the oceanic lithosphere, although the thickness and depletion degree of the chemical mantle lithosphere is determined by the ambient mantle temperature. The thermal lithosphere can be thinner or thicker, because of different cooling ages before subduction. We test different thermal thickness between 50-150 km, so as to cover a large value ranges. The temperature increases linearly with depth to the bottom of the thermal lithosphere, where it is equal to the temperature value of the ambient mantle.

The temperature field for the continental blocks increases linear from surface to the Moho then increases linear from Moho to the thermal LAB, where it is also equal to the temperature value of the ambient mantle. The Moho temperature in all the models here are set to ~ 450 ºC at their initial steps. This geotherm profile is close to those calculated from geothermobarometric data of xenoliths (Lee et al., 2011 and references therein).

F_b in Eq. 2 can be described as a function of ρ, Tp and model time (t):

$$F_b = -\left(\rho - \rho_{ref(depth)}\left(1 - \alpha\Delta Tp(1 - \frac{t}{2500\ Myr})\right)\right)g \quad (15)$$

Model setups

To reproduce the Archean slab stacking behavior revealed by previous studies (Calvert et al., 1995; Helmstaedt and Schulze, 1986; Kusky, 1993), a subduction-collision-post collision tectonic process is designed for all the numerical models here, with two convergent plates overlying an Archean ambient mantle (with different adiabats, ΔTp=135-250 K in different models) (Aulbach and Arndt, 2019; Ganne and Feng, 2017; Herzberg et al., 2010). The model domain is 3000 km wide and 700 km deep, with 10×10 km resolution. The pro-plate contains a leading oceanic slab and a trailing cratonic block, whereas the retro-plate contains only a cratonic block. The cratonic blocks are composed of upper crust, lower crust and chemically buoyant CLM, whereas the oceanic slab contains a crustal layer and a chemically buoyant peridotite layer. The thickness of the oceanic crust and the depletion degree of oceanic mantle lithosphere are described above. The depletion degree of CLM is modeled as a function of depth as constrained by previous works (Bernstein et al., 2007; O'Reilly and Griffin, 2006).

The upper and side boundaries are free slip, lower boundary is open. The initial temperature field is shown in Fig. S2, in which the upper boundary has fixed temperature and the lower boundary has a linearly decreasing temperature with time as mentioned above.

In different model setups, we mainly change the mantle temperature (ΔTp), slab thermal thickness (or ages), convergence rate, stacking dip angle, strength factors of peridotite and eclogite in different models (Table S2), to investigate the influences of these parameters on model evolutions.

The ΔTp and slab thermal thickness are discussed above. The convergence rate in the Archean is not well constrained, thus we test a large value range from 1.0-10.0 cm/yr. Subduction angles in the Archean are suggested to be on average lower than the present

ones because higher average lithosphere depletion degrees induce greater buoyancy (Abbott et al., 1994); however, there is no evidence to exclude steep and deep subduction in the early times (Agrusta et al., 2018; Windley et al., 2021), and some evidence that subduction reached 270 and perhaps 660 km (Kusky et al., 2021). Given these uncertainties, we test modes with different stacking dip angles between 15-45°. The subducted crustal and slab mantle materials are likely weaker than their dry undeformed equivalents because of possible existences of hydroweakening, strain-weakening, partial melting, and recrystallization related grain-size reduction (Hirth and Kohlstedt, 2003; Zhang and Green, 2007). Thus, we designed different models with different strength factors for the crustal and slab mantle materials.

Postprocessing

To calculate the volume fraction of eclogite at different depth intervals ($X_{\text{eclogite @ depth interval}}$), the volume fraction of eclogite is calculated first in each finite element cell ($X_{\text{eclogite in cell}}$), via the equation below, to form a cell-based average eclogite volume fraction:

$$X_{eclogite\ in\ cell} = \frac{eclogite\ particle\ number\ in\ cell}{total\ particle\ number\ in\ cell} \tag{16}$$

Then the volume fraction at each depth intervals is further averaged at the related depth interval, based on this cell-based average value:

$$X_{eclogite\ @\ depth\ interval} = \frac{\sum X_{eclogite\ in\ cell} @ depth\ interval}{cell\ number @ depth\ interval} \tag{17}$$

We take depth intervals equal to the element cell size (10 km) to get the related results in Figure 2, 3, 4 in the main text.

Supplemental Figures

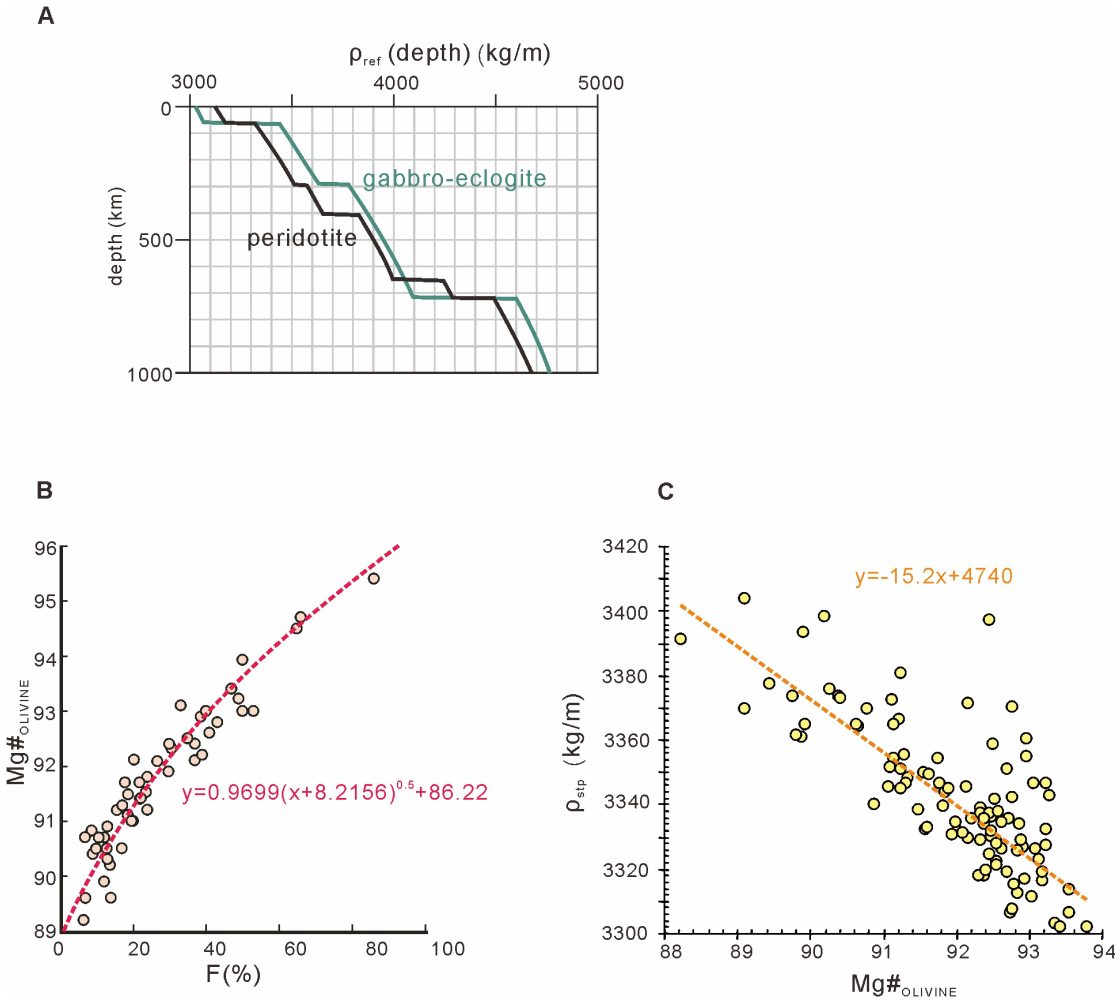

Fig. S1. Density parameters of peridotites and eclogites. (A) Reference density vs. depth along the present mantle adiabat. **(B)** $Mg\#_{OLIVINE}$ can be approximately deemed as a function of F (Bernstein et al., 2007). **(C)** ρ_{stp} is a function of $Mg\#_{OLIVINE}$ (Lee, 2003). Thus, ρ_{stp} can be deemed as a function of F, that is $\rho_{stp(F)}$.

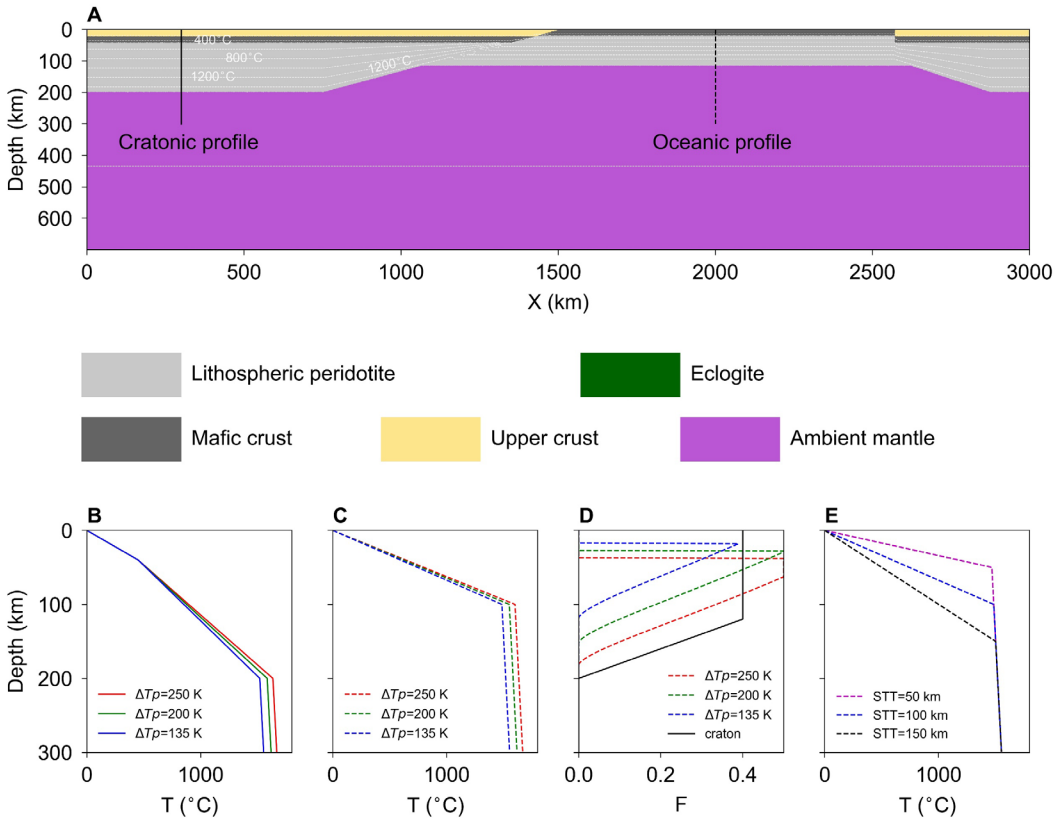

Fig. S2. Initial conditions for different model setups. (A) Material and temperature fields. (B) Temperature profile of cratonic domains above different Archean ambient mantle (ΔTp=135-250 K). (C) Temperature profile of oceanic domains above different Archean ambient mantle (ΔTp=135-250 K). (D) Depletion profile of oceanic domains related to ΔTp=135-250 K, and cratonic domains according to references (Bernstein et al., 2007; O'Reilly and Griffin, 2006). (E) Temperature profile of oceanic domains influenced by different slab thermal thickness (slab thermal lithosphere-asthenosphere boundary, STLAB=50-150 km).

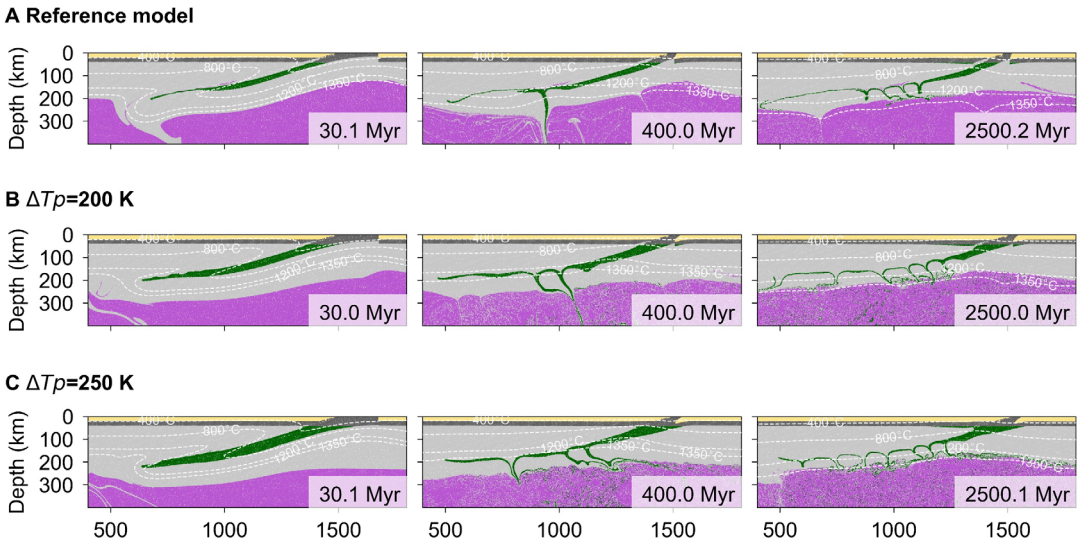

Fig. S3. Influences of mantle potential temperature ΔTp. (A) ΔTp=135 K. (B) ΔTp=200 K. (C) ΔTp=250 K.

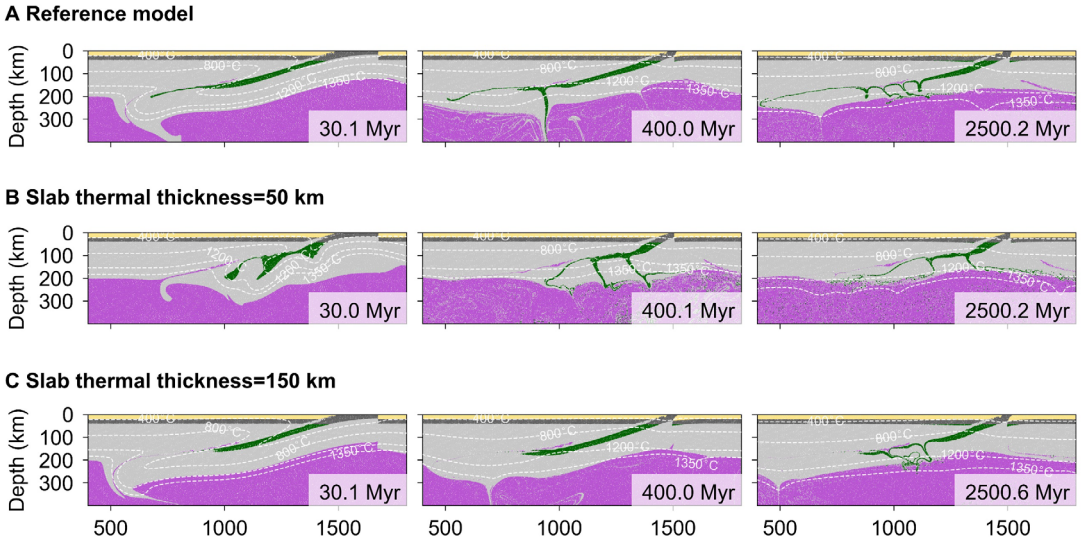

Fig. S4. Influences of slab thermal thickness. (A) slab thermal thickness=100 km. (B) slab thermal thickness=50 km. (C) slab thermal thickness=150 km.

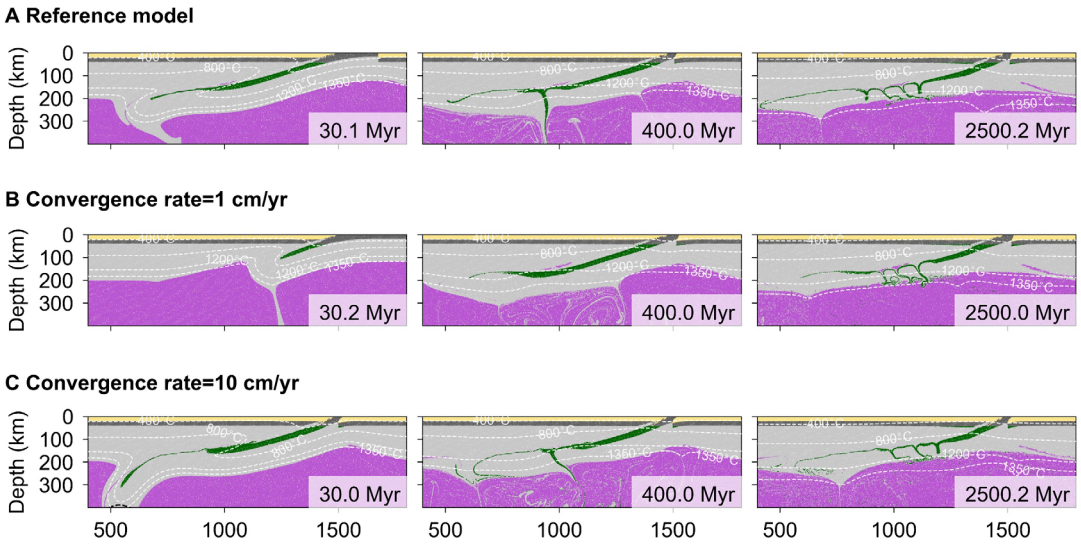

Fig. S5. Influences of convergence rate. (A) convergence rate=3 cm/yr. (B) convergence rate=1 cm/yr. (C) convergence rate=10 cm/yr

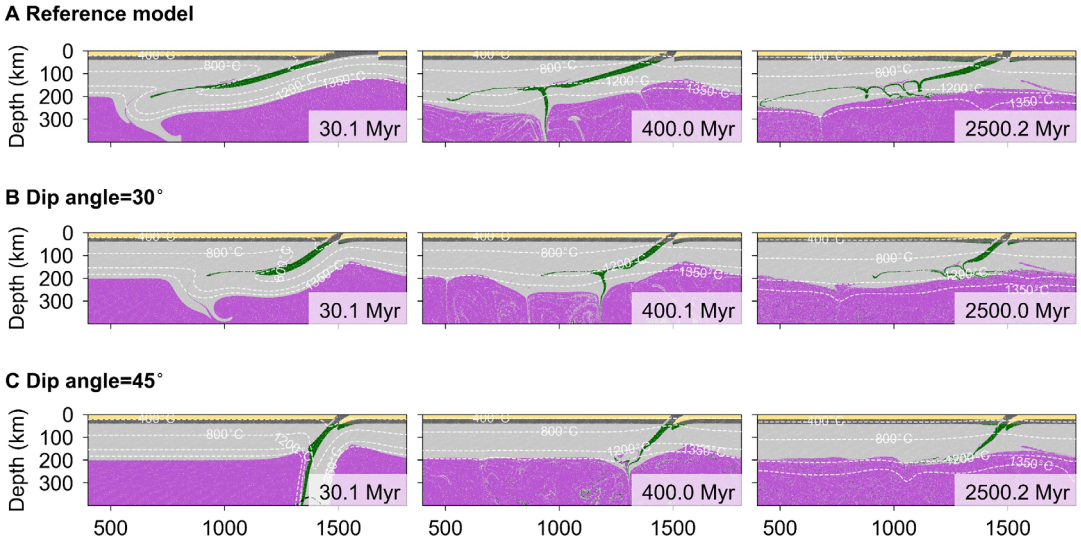

Fig. S6. Influences of stacking dip angle. (A) dip angle=15°. (B) dip angle=30°. (C) dip angle=45°.

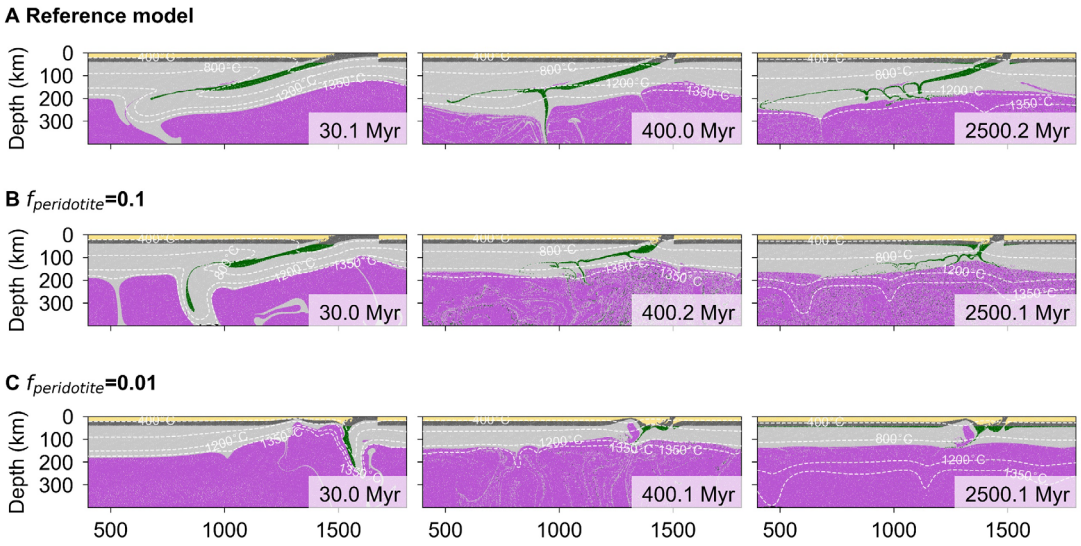

Fig. S7. Influences of CLM peridotite strength factor ($f_{peridotite}$). (A) $f_{peridotite}$=1.0. (B) $f_{peridotite}$=0.1. (C) $f_{peridotite}$=0.01.

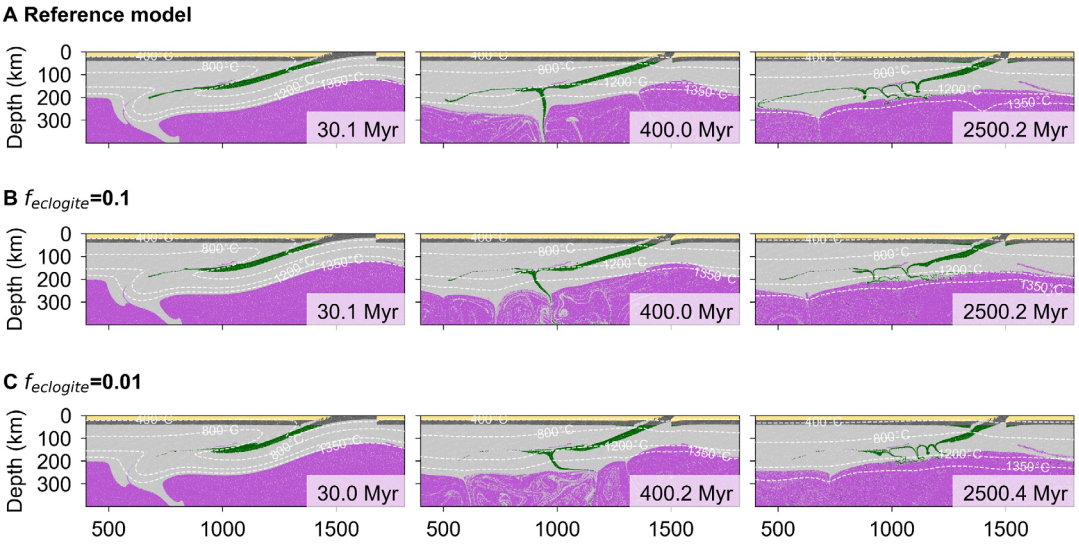

Fig. S8. Influences of CLM eclogite strength factor ($f_{eclogite}$). (A) $f_{eclogite}$=1.0. (B) $f_{eclogite}$=0.1. (C) $f_{eclogite}$=0.01.

Supplemetnal Tables

Table S1. Model parameters.

Symbol	Meaning	Dry peridotites	Eclogites	Upper crust	Lower/Oceanic crust	Units
A_{diff}	Pre-exponential parameter of diffusion creep	1.0×10^{9}	-		-	$Pa^{-1} \cdot S^{-1}$
A_{disl}	Pre-exponential parameter of dislocation creep	5.209×10^{4}	1.0701×10^{5}	3.3497×10^{8}	1.404×10^{3}	$Pa^{-n} \cdot S^{-1}$
E_{diff}	Activation energy of diffusion creep	3.35×10^{5}	-		-	$J \cdot mol^{-1}$
E_{disl}	Activation energy of dislocation creep	4.8×10^{5}	4.8×10^{5}	1.38×10^{5}	4.97×10^{5}	$J \cdot mol^{-1}$
V_{diff}	Activation volume of diffusion creep	4.0×10^{-6}	-	-	-	$m^{3} \cdot mol^{-1}$
V_{disl}	Activation volume of dislocation creep	11×10^{-6}	0	0	0	$m^{3} \cdot mol^{-1}$
n	Power-law exponent	3.5	3.4	3.4	3.4	-
C0	Cohesion	1×10^{7}	1×10^{7}	1×10^{7}	1×10^{7}	Pa
C1	Sine of internal frictional angle	0.6	0.6	0.6	0.6	S^{-1}
ρ_0	Reference density at 273.15 K, 0 Pa	-	-	2600	-	$kg \cdot m^{-3}$
$Q_{present}$	Present radiogenic heating	0.022	0.5	2.0	0.5	$\mu W \cdot m^{-3}$

Thermal diffusion (1×10^{-6} m^2/s), specific heat (1300 J/kg/K), thermal expansion coefficient (3×10^{-5} K^{-1}), compressibility (1×10^{-11} Pa^{-1}), and Heat production (0 μW m-3) are set to be fixed for different rocks. Rheological parameters of peridotites (Čížková et al., 2012), eclogites (Jin et al., 2002), upper crust (dry granite) (Hansen, 1982) and lower/oceanic crust (dry gabbro) (Wilks and Carter, 1990) are from previous studies. Radiogenic heating data is from Turcotte and Schubert (2002)

Table S2. Model runs.

	ΔTp (K)	Slab thermal thickness (km)	Convergence rate (cm/yr)	Dip angle (degree)	f of CLM peridotites	f of Eclogite
Run 0 (Reference model)	135	100	3	15	1.0	1.0
Run 1	**200**					
Run 2	**250**					
Run 3		50				
Run 4		150				
Run 5			1			
Run 6			5			
Run 7			10			
Run 8				30		
Run 9				45		
Run 10					**0.1**	
Run 11					**0.01**	
Run 12						**0.1**
Run 13						**0.01**

Blank space indicate the values are consistent with the related ones in the reference model (Run0).

References

Abbott, D., Drury, R., and Smith, W.H., 1994, Flat to steep transition in subduction style: Geology, v. 22, p. 937-940.

Agrusta, R., van Hunen, J., and Goes, S., 2018, Strong plates enhance mantle mixing in early Earth: Nature Communications, v. 9, p. 2708.

Aulbach, S., and Arndt, N.T., 2019, Eclogites as palaeodynamic archives: Evidence for warm (not hot) and depleted (but heterogeneous) Archaean ambient mantle: Earth and Planetary Science Letters, v. 505, p. 162-172.

Bernstein, S., Kelemen, P.B., and Hanghøj, K., 2007, Consistent olivine Mg# in cratonic mantle reflects Archean mantle melting to the exhaustion of orthopyroxene: Geology, v. 35, p. 459–462.

Calvert, A.J., Sawyer, E.W., Davis, W.J., and Ludden, J.N., 1995, Archaean subduction inferred from seismic images of a mantle suture in the Superior Province: Nature, v. 375, p. 670-674.

Capitanio, F.A., Nebel, O., and Cawood, P.A., 2020, Thermochemical lithosphere differentiation and the origin of cratonic mantle: Nature, v. 588, p. 89-94.

Čížková, H., van den Berg, A.P., Spakman, W., and Matyska, C., 2012, The viscosity of Earth’s lower

mantle inferred from sinking speed of subducted lithosphere: Physics of the earth and Planetary Interiors, v. 200, p. 56-62.

Ganne, J., and Feng, X., 2017, Primary magmas and mantle temperatures through time: Geochemistry, Geophysics, Geosystems, v. 18, p. 872-888.

Hansen, F.D., 1982, Semibrittle creep of selected crustal rocks at 1000 MPa (Ph. D Dissertation): College Station, Texas, Texas A & M University.

Helmstaedt, H., and Schulze, D.J., 1986, Southern African kimberlites and their mantle sample: Implications for Archean tectonics and lithosphere evolution, Geological Society of Australia, Special Publication.

Herzberg, C., Condie, K., and Korenaga, J., 2010, Thermal history of the Earth and its petrological expression: Earth and Planetary Science Letters, v. 292, p. 79-88.

Herzberg, C., and Rudnick, R., 2012, Formation of cratonic lithosphere: an integrated thermal and petrological model: Lithos, v. 149, p. 4-15.

Hirth, G., and Kohlstedt, D., 2003, Rheology of the upper mantle and the mantle wedge: A view from the experimentalists: Inside the subduction Factory, v. 138, p. 83-105.

Jin, Z.M., Zhang, J., Green, H.W.I., and Jin, S., 2002, Eclogite rheology: Implications for subducted lithosphere: Geology, v. 29, p. 667-670.

Katz, R.F., Spiegelman, M., and Langmuir, C.H., 2003, A new parameterization of hydrous mantle melting: Geochemistry, Geophysics, Geosystems, v. 4.

Kusky, T., Wang, L., Robinson, P.T., Huang, Y., Wirth, R., Ning, W., Zhong, Y., and Polat, A., 2021, Ultra-high pressure inclusion in Archean ophiolitic podiform chromitite in mélange block suggests deep subduction on early Earth: Precambrian Research, v. 362, p. 106318.

Kusky, T.M., 1993, Collapse of Archean orogens and the generation of late-to postkinematic granitoids: Geology, v. 21, p. 925-928.

Lee, C.A., 2003, Compositional variation of density and seismic velocities in natural peridotites at STP conditions: Implications for seismic imaging of compositional heterogeneities in the upper mantle: Journal of Geophysical Research: Solid Earth, v. 108.

Lee, C.A., Luffi, P., and Chin, E.J., 2011, Building and destroying continental mantle: Annual Review of Earth and Planetary Sciences, v. 39, p. 59-90.

Moresi, L., Dufour, F., and Mühlhaus, H., 2003, A Lagrangian integration point finite element method for large deformation modeling of viscoelastic geomaterials: Journal of Computational Physics, v. 184, p. 476-497.

O'Reilly, S.Y., and Griffin, W.L., 2006, Imaging global chemical and thermal heterogeneity in the subcontinental lithospheric mantle with garnets and xenoliths: Geophysical implications: Tectonophysics, v. 416, p. 289-309.

Ranalli, G., 1995, Rheology of the Earth, Deformation and Flow Processes in Geophysics and Geodynamics, second ed. Chapman & Hall.

Rodríguez González, J., Negredo, A.M., and Billen, M.I., 2012, The role of the overriding plate thermal state on slab dip variability and on the occurrence of flat subduction: Geochemistry, Geophysics,

Geosystems, v. 13, p. doi:10.1029/2011GC003859.

Turcotte, D.L., and Schubert, G., 2002, Geodynamics, Cambridge University Press.

Wang, H., van Hunen, J., and Pearson, D.G., 2018, Making Archean cratonic roots by lateral compression: A two-stage thickening and stabilization model: Tectonophysics, v. 746, p. 562-571.

Wilks, K.R., and Carter, N.L., 1990, Rheology of some continental lower crustal rocks: Tectonophysics, v. 182, p. 57-77.

Windley, B.F., Kusky, T., and Polat, A., 2021, Onset of plate tectonics by the Eoarchean: Precambrian Research, v. 352, p. 105980.

Xu, W., Lithgow-Bertelloni, C., Stixrude, L., and Ritsema, J., 2008, The effect of bulk composition and temperature on mantle seismic structure: Earth and Planetary Science Letters, v. 275, p. 70-79.

Yan, J., Ballmer, M.D., and Tackley, P.J., 2020, The evolution and distribution of recycled oceanic crust in the Earth's mantle: Insight from geodynamic models: Earth and Planetary Science Letters, v. 537, p. 116171.

Zhang, J., and Green, H.W., 2007, Experimental Investigation of Eclogite Rheology and Its Fabrics at High Temperature and Pressure: Journal of Metamorphic Geology, v. 25, p. 97 – 115.